

Studying the Kinetics of a Self-propelled Cruiser in 2D Granular Media under Gravity

Guo-Jie J. Gao^{1,*}

¹*Department of Mathematical and Systems Engineering,
Shizuoka University, Hamamatsu, Shizuoka 432-8561, Japan
(Dated: September 18, 2018)*

We propose a cruiser able to move in a granular medium made of nearly 50-50 bidisperse dissipative particles under gravity. The cruiser has a circular shape with a square indentation on its edge. By shifting and then ejecting granular particles entering its indent-region facing a given direction, the cruiser gains thrust to push itself forward in the same direction, which can be either perpendicular or parallel to gravity. Using molecular dynamics (MD) simulations, we identify three universal phases during one particle-ejection process: 1) acceleration by the ejection thrust, 2) deceleration by the compressed particles ahead and 3) relaxation with the decompressed particles. We also confirm that the cruising capability improves with increasing the particle-ejection strength and with decreasing the interference from gravity.

I. INTRODUCTION

Designing and analyzing self-propelled machines in thermal fluids such as air and water can be dated back to the beginning of recorded history. The equilibrium characteristics of thermal fluids allow us to easily understand their physical properties and explore their interactions with objects inside them both microscopically and macroscopically. However, similar endeavors to study mobile machines in athermal fluids such as nonequilibrium granular materials have been initiated only recently [1], mainly because the nonequilibrium features make developing a governing equation of the system a challenging task [2]. Among the finite attempts tackling this challenge in the literature, except some artificial designs [3–8], most of them are bio-inspired, such as mimicking sandfish, lizard and snake [4, 9–15], insects [16] and clam that uses an intricate way to move forward by swallowing and discharging sands [17, 18]. Learning from the nature has the benefit of always having an original counterpart that has been optimised through long evolution to compare with, and the mimicked designs are guaranteed to function under known conditions. Nevertheless, the bio-inspired designs have their limitation. Sometime to achieve better motion efficiency or controllability, one needs to introduce mechanical components that do not exist in living creatures such as installing a propeller or a compressor on a glider imitating a bird initially.

In this study, we propose an extremely simple and novel design of a self-propelled cruiser, able to move freely in a 2D granular medium made of bidisperse dissipative particles under gravity. The cruiser has a circular shape plus a square indentation of finite size on its edge. To move into a given direction, the cruiser directs its indentation facing the moving direction, shifts any particles entering the indentation to its rear-half part and ejects the shifted particles backward to gain forward thrust. Through successive ejections, the cruiser can propel it-

self and travel within the granular medium either perpendicular or parallel to gravity. Using molecular dynamics (MD) methods, we test the kinetic response of the cruiser under different ejection strengths and study its maneuverability within frictionless bidisperse particles with damping. We identify three distinct and universal phases during one particle-ejection: 1) obtaining momentum from the ejected particles, 2) proceeding due to the inertial effects and 3) relaxing with the rebounding particles compressed ahead. Moreover, we also confirm that the cruiser can move further proportional to the ejection strength. Finally, cruising against or with gravity reduces the propelling efficiency.

Below we elaborate on the details of the simulated system and the design of our self-propelled cruiser in section II, followed by quantitative analysis of its ejection kinetics and cruising capability under different simulation setups in section III. We conclude our study in section IV.

II. NUMERICAL SIMULATION METHOD

A. Preparing a non-overlapped initial configuration

Using molecular dynamics (MD) method, we study the kinetics of a self-propelled cruiser moving in a granular medium of nearly 50-50 bidisperse frictionless circular dry particles with damping in a square container of size L , as shown in Fig. 1(a).

To prepare a non-overlapped initial configuration for the MD simulation, in the square container initially we randomly place N_s small discs and N_l large discs of diameters d_s and d_l , respectively, determined by $\phi = (\pi/4L^2)(N_s d_s^2 + N_l d_l^2) = 0.833$, and $N_{tot} = N_s + N_l = 4096$. This gives $d_s \approx 0.0132L$. We keep the diameter ratio d_l/d_s between large and small discs at 1.4 to prevent artificial crystallization in a two dimensional environment.

Then we insert a circular cruiser of radius $R = 0.1L$ with a finite-sized square indentation of size $\Delta = 2d_s$ on its edge into the container and remove all granular

* koh.kokketsu@shizuoka.ac.jp, gjgao@gmail.com

particles within a circular range R from the center of the cruiser. On average, this removes about $100 \sim 200$ particles from the container and evenly reduces N_s and N_l , which produces a nearly 50-50 bidisperse system, and N_{tot} becomes slightly less than 4000.

Finally, to quickly remove all inter-particle overlaps in the system, we perform MD simulations under zero gravity by introducing a finite-range, pairwise purely repulsive linear spring force $\vec{f}_{ij}^n(r_{ij})$ and minimizing the total normal force on each object in the system, where the normal interaction between any two objects i and j (particle-particle or particle-cruiser) is governed by

$$\vec{f}_{ij}^n(r_{ij}) = \frac{\epsilon}{d_{ij}^2} \delta_{ij} \Theta(\delta_{ij}) \hat{r}_{ij}, \quad (1)$$

where r_{ij} is the separation between objects i and j , ϵ is the characteristic elastic energy scale, $d_{ij} = (d_i + d_j)/2$ is the average size of objects i and j , $\delta_{ij} = d_{ij} - r_{ij}$ is the inter-object overlap, $\Theta(x)$ is the Heaviside step function, and \hat{r}_{ij} is the unit vector connecting the centers of the two objects. When approaching a wall, a particle feels its identical image with the same relative distance on the other side of the wall.

B. System setup for cruising under gravity

1. Forces on a granular particle

In the simulation under nonzero gravity, each frictionless particle i obeys Newton's translational equation of motion

$$\vec{F}_i = \vec{F}_i^{\text{int}} + \vec{F}_i^W + \vec{F}_i^C + \vec{F}_i^G = m_i \vec{a}_i, \quad (2)$$

where \vec{F}_i is the total force acting on particle i with mass m_i and acceleration \vec{a}_i . \vec{F}_i^{int} , \vec{F}_i^W , \vec{F}_i^C and \vec{F}_i^G are forces acting on the particle from its contact neighbors, the container walls, the cruiser and gravity, respectively. Below we elaborate on each of these terms individually.

To simulate frictionless granular materials, we consider only the interparticle normal forces for simplicity reason [19]. The interparticle force \vec{F}_i^{int} on particle i having N_c contact neighbors j can be expressed as

$$\vec{F}_i^{\text{int}} = \sum_{j \neq i}^{N_c} [\vec{f}_{ij}^n(r_{ij}) + \vec{f}_{ij}^d(r_{ij})], \quad (3)$$

where $\vec{f}_{ij}^n(r_{ij})$ is the interparticle normal force, having the same form defined in Eqn.(1), and $\vec{f}_{ij}^d(r_{ij})$ is the interparticle normal damping force defined in Eqn.(4) below. We consider the interparticle normal damping force proportional to the relative velocity between particles i and j

$$\vec{f}_{ij}^d(r_{ij}) = -b \Theta(\delta_{ij}) (\vec{v}_{ij} \cdot \hat{r}_{ij}) \hat{r}_{ij}, \quad (4)$$

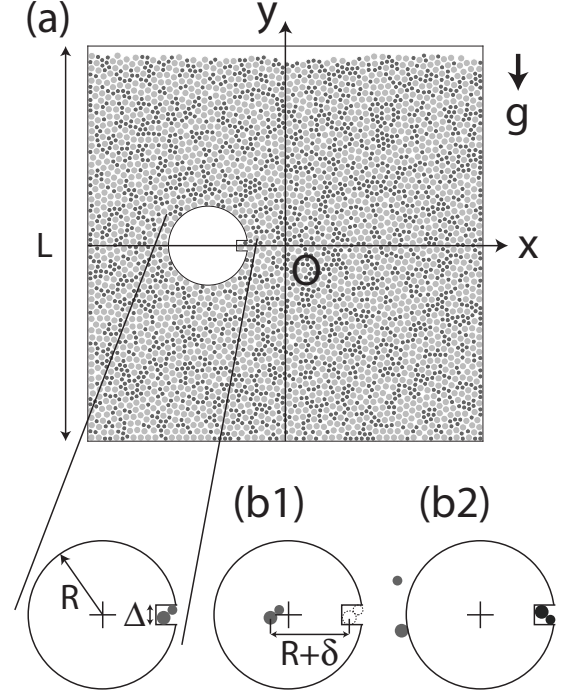


FIG. 1. (Color online) (a) The MD simulation setup of a square container of size L , storing about 4000 bidisperse dissipative particles and a circular cruiser under gravity g . The small (dark grey) and large (light grey) particles measure d_s and d_l in diameter, separately, with a size ratio of 1.4. The blowup shows the cruiser, having a radius R and an square indentation of size $\Delta = 2d_s$ on its edge. The cruiser shifts particles entering its square indent-region to its rear by a distance of $R + \delta$ and ejects them backward to gain thrust for moving forward, as shown in (b1) and (b2), respectively.

where b is the damping parameter, \vec{v}_{ij} is the relative velocity between the two particles. The normal damping force results in deduction of the kinetic energy of the involved particles after each pairwise collision.

The interaction force \vec{F}_i^W between particle i and a container wall has an analogous form to the interparticle normal interaction \vec{f}_{ij}^n , except with $\epsilon^W = 2\epsilon$, which means when a particle hits a wall, it experiences a repulsive force as if it hit another mirrored self on the other side of the wall. \vec{F}_i^W can include contributions from multiple walls: for example, a particle can sit at the corner formed by two perpendicular walls.

The particle-cruiser interaction force \vec{F}_i^C can be expressed as

$$\vec{F}_i^C = \vec{f}_{iC}^n + \vec{f}_{iC}^d, \quad (5)$$

where \vec{f}_{iC}^n and \vec{f}_{iC}^d are the particle-cruiser normal force and normal damping force, respectively. If a particle touches the circular edge of the cruiser, $\vec{f}_{iC}^n = \vec{f}_{ij}^n$, and

\vec{f}_{iC}^d is zero. Otherwise, if a particle touches the walls of the square indentation of the cruiser, $\vec{f}_{iC}^n = \vec{F}_i^W$ and $\vec{f}_{iC}^d = \vec{f}_{ij}^d$, except with a much larger damping parameter $b_C = 50b$. The large b_C helps the cruiser to keep granular particles within its square indent-region once they enter it.

Finally, $\vec{F}_i^G = -m_i g \hat{y}$, where g is the gravitational constant, and \hat{y} is the unit vector in the upward direction. There is no tangential interaction on frictionless particles in this model, and therefore Newton's rotational equation of motion is automatically satisfied.

2. Forces on the cruiser

Based on Newton's translational equation of motion, the total force \vec{F}_C acting on the cruiser with mass m_C and acceleration \vec{a}_C , in contact with N_p particles, is

$$\vec{F}_C = \left(-\sum_i^{N_p} \vec{F}_i^C\right) + \vec{F}_C^G = m_C \vec{a}_C, \quad (6)$$

where the minus sign in front of \vec{F}_i^C comes from Newton's third law of motion, and $\vec{F}_C^G = -m_C g \hat{y}$. In this study, we do not perform simulations where the cruiser can touch the container wall, so the cruiser-wall interaction can be safely ignored.

We also do not consider Newton's rotational equation of motion of the cruiser by redefining the indent-region of the cruiser according to its center position at each MD step. This approach causes the cruiser to drift slightly if any particle interacts with the indentation walls of the cruiser. The drifting effect is not significant, because at most only two or three particles can enter the indent-region based on our MD simulation results. Besides, in the MD simulations, the mass of an object is proportional to its area size, meaning the cruiser is about 229 or 117 times heavier than a small or large granular particle. The above two reasons justify this approach, so we can focus only on the translational motion of the cruiser.

3. Reference scales and simulation parameters

The MD simulations in this study use the diameter d_s and mass m_s of the small particles and the interparticle elastic potential amplitude ϵ as the reference length, mass, and energy scales, respectively. We choose the dimensionless damping parameter $b^* = db/\sqrt{m\epsilon} = 0.5$, the dimensionless gravity $g^* = 10^{-3}$, and a dimensionless time step $dt^* = dt/d\sqrt{m/\epsilon} = 10^{-2}$ throughout this study.

4. Relaxation of the non-overlapped initial configuration

After generating a non-overlapped initial configuration, we relax it under nonzero gravity. To do this, we monitor the relative error η of the total potential energy of the system $V_{tot} = V^{int} + V^W + V^G$ between time t and $t + \Delta t$, where V^{int} is the total repulsive linear spring potential between objects, V^W is the total repulsive linear spring potential between particles and walls, V^G is the total gravitational potential in the system, based on the forces given in section IIB 1 and section IIB 2, and $\Delta t = 1000$. We terminate the relaxation when $\eta(V_{tot}) < 10^{-5}$. A relaxed initial configuration and the cruiser with a radius R and a square indentation of size $\Delta = 2d_s$, are shown in Fig. 1(a).

C. Ejection mechanism of the cruiser

The ejection mechanism of the cruiser can be divided into two steps: 1) The cruiser detects if there are particles whose centers are within the pocket region of its square indentation. If the answer is yes, those particles will be shifted horizontally or vertically by a distance $R + \delta$ away from the indentation, as depicted in Fig. 1(b1). δ is a control parameter in this study. This shift of pocketed particles has twofold important purpose in the coming relaxation step: First, we store spring potential energy between the shifted particles and the cruiser, which will transform into work and supply thrust to push the cruiser forward. Second, the emptied indent-region offers necessary space to unjam the region ahead of the cruiser a bit, so that the cruiser can proceed. 2) Using the stored potential energy, the cruiser ejects the shifted particles backward and obtain thrust to propel itself forward. The thrust has the same form as \vec{f}_{ij}^n , defined in Eqn.(1). We do not strictly control the ejection directions of the shifted particles and let \vec{f}_{ij}^n be in charge of the process automatically. The second step is done by a full relaxation of the system, terminated at $\eta(V_{tot}) < 10^{-5}$. During the relaxation, New particles can enter the pocket region of the indentation and stay there after the relaxation ends, as shown in Fig. 1(b2). The ejected particles also prevent the cruiser from receding. By repeating the above two steps, the cruiser can transit in the bidisperse granular medium under systematic control.

III. RESULTS AND DISCUSSIONS

Below we investigate the kinetics of three different particle-ejection modes of the cruiser: 1) perpendicular to gravity, 2) against gravity and 3) with gravity, followed by an analysis of the averaged performance of the cruiser if it ejects pocketed-particles successively in each mode at different ejection strength.

A. Particle-ejection perpendicular to gravity

To study the kinetic response of the horizontal particle-ejection mode perpendicular to gravity, initially we place the cruiser at $(x, y) = (-0.2L, 0.0)$ in the container and put the square indentation facing the moving direction along the horizontal axis. After the first relaxation, several particles enter the square indent-region of the cruiser, and then we shift them horizontally by a distance of $R + \delta$ away from the indentation, as depicted in Fig. 1(b1). We vary the value of δ from $0.5d_s$, $2.0d_s$ to $3.5d_s$ and measure the total force F_C^x on the cruiser, its velocity component perpendicular to gravity V_C^x and its normalized horizontal displacement $(X_C - X_C^0)/d_s$ when the cruiser ejects the shifted particles in the second relaxation. In Fig. 2, we show these quantities from an exemplary case as a function of time t , where exactly two particles are ejected by the cruiser. We can separate the time series into three phases, I, II, and III as follows.

Phase I in Fig. 2(a) shows that initially F_C^x decreases monotonically and smoothly from a high value, when the shifted particles are just being ejected from the cruiser, to a nearly zero value, when they completely disengage from it. In this phase, the cruiser picks up speed, and V_C^x increases and eventually reaches its maximum, as shown in Fig. 2(b). V_C^x cannot increase anymore after phase I, because the ejected particles have no more overlap with the cruiser and therefore can supply no more thrust. The corresponding $(X_C - X_C^0)/d_s$, however, only increases slightly, as shown in Fig. 2(c). This also justifies the nearly zero F_C^x mentioned above.

Next, in phase II, the cruiser keeps moving forward due to inertial effects, using the momentum built up in the previous phase. The forward-going cruiser keeps pressing the particles ahead, which cause F_C^x on the cruiser to become negative and against its motion, and eventually the negative F_C^x stops the cruiser. Nevertheless, it is in this phase when new particles, used for next particle-ejection, enter the indent-region, and the cruiser gains most of its forward displacement among all three phases.

Finally, in phase III, the cruiser already exhausts most of its momentum and the compressed particles ahead of it start to push back. We can observe that the compressed particles decompress themselves through a series of intermittent negative impulses. Each of these impulses is not strong enough to push the cruiser back substantially, and the cruiser never regain considerable momentum as in phase I. The occasionally increased kinetic energy in the system due to an impulse is quickly dissipated through interparticle damping forces. Therefore, V_C^x only fluctuates around zero. Until the end of the relaxation, the accumulated backward movement is still not large enough to send the cruiser back to where it started. The net effect on $(X_C - X_C^0)/d_s$ is that the cruises can proceed by this 'one steps forward, half step back' strategy. As we reduce the ejection strength δ from $0.5d_s$, $2.0d_s$ to $3.5d_s$, the responses of all three quantities diminish systematically, but all trends discussed above stay unchanged.

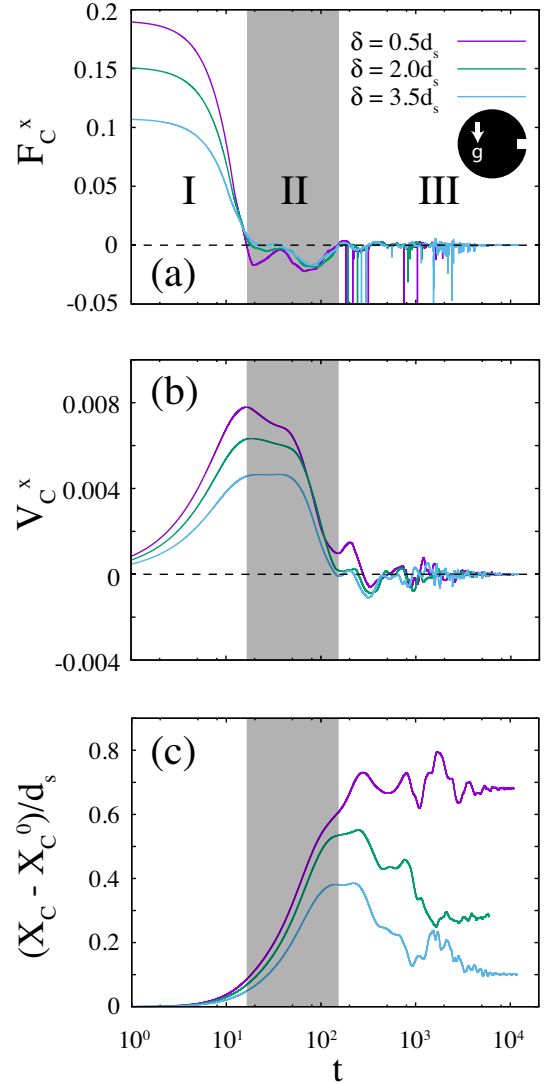


FIG. 2. (Color online) The x components of (a) total force F_C^x on the cruiser, (b) its velocity V_C^x and (c) its net displacement $(X_C - X_C^0)/d_s$, normalized by the small particle diameter d_s , during a single ejection of exactly two particles, perpendicular to gravity, as a function of the shift distance $\delta = 0.5d_s$ (dark), $2.0d_s$ (medium) and $3.5d_s$ (light), respectively. The particle-ejection strength is inversely proportional to δ . The cruiser is initially placed at $(x, y) = (-0.2L, 0.0)$ with its indentation pointing horizontally. The ejection process can be divided into three phases, I, II and III, as discussed in the text.

B. Particle-ejection against or with gravity

Similarly, to study the kinetics of the vertical particle-ejection mode against or with gravity, initially we place the cruiser at $(x, y) = (0.0, -0.2L)$ or $(x, y) = (0.0, 0.2L)$ in the container and put the square indentation on top of or at the base of the cruiser along the vertical axis. Likewise, the behavior of F_C^y , V_C^y and $(Y_C - Y_C^0)/d_s$ as a function of time t from exemplary cases, where exactly

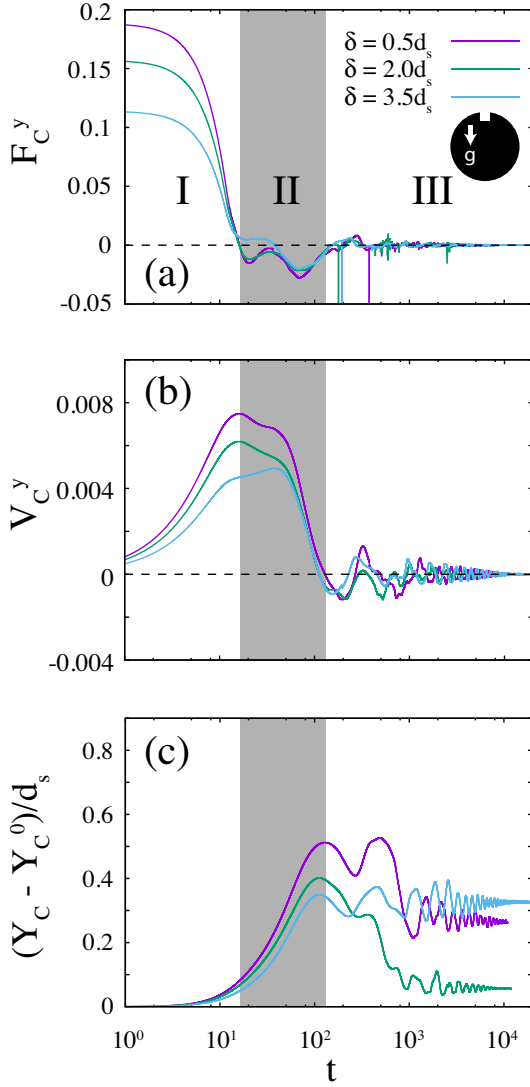


FIG. 3. (Color online) The y components of (a) total force F_C^y on the cruiser, (b) its velocity V_C^y and (c) its net displacement $(Y_C - Y_C^0)/d_s$, normalized by the small particle diameter d_s , during a single ejection of exactly two particles against gravity, as a function of the shift distance $\delta = 0.5d_s$ (dark), $2.0d_s$ (medium) and $3.5d_s$ (light), respectively. The cruiser is initially placed at $(x, y) = (0.0, -0.2L)$ with its indentation placed on the top of the cruiser. The ejection process can also be divided into three phases, I, II and III, as in Fig. 2.

two particles are ejected by the cruiser, are shown in Fig. 3 and Fig. 4 for tests against gravity and with gravity, respectively.

Basically, for each ejection mode, we observe similar patterns in all three phases as those shown in the horizontal ejection mode, except two new things to notice. First, in phase II, when the ejection mode is in line with gravity, gravity also contributes to accelerate the cruiser, and therefore the cruiser gains higher maximum velocity $|V_C^y|$ than ejection against gravity, as can be seen in Fig. 3(b) and Fig. 4(b). Second, as expected, gravity makes

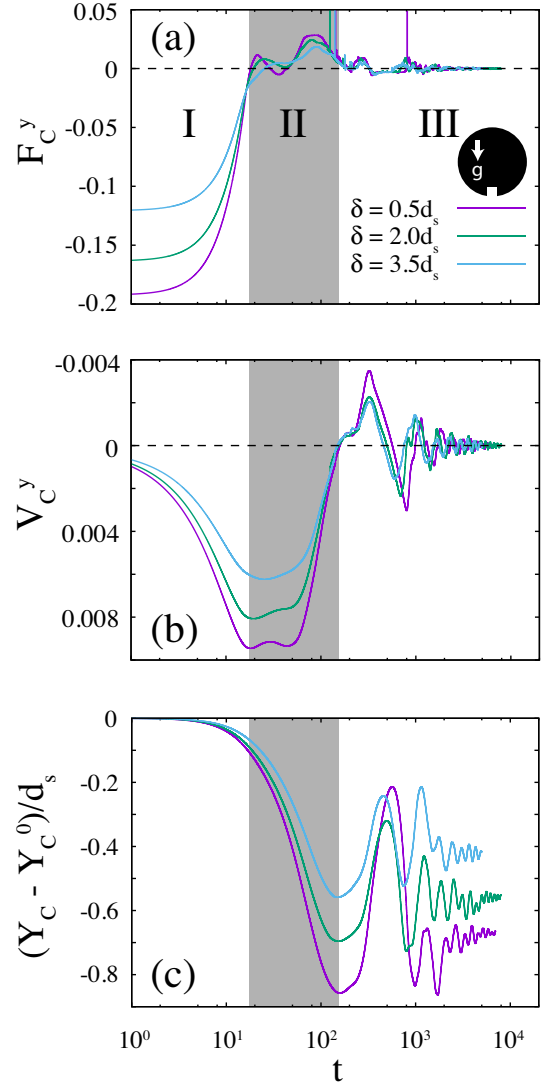


FIG. 4. (Color online) Same quantities as in Fig. 3 during a single ejection with gravity. The cruiser is initially placed at $(x, y) = (0.0, 0.2L)$ with its indentation placed at the bottom of the cruiser.

$(Y_C - Y_C^0)/d_s$ oscillate more obviously in phase III in both vertical ejection modes, as shown in Fig. 3(c) and Fig. 4(c), which is less noticeable in the horizontal ejection mode.

C. Cruising capability by successive particle-ejection

To evaluate the cruising capability when the cruiser successively ejects particles entering its square indentation, we prepare ten different initial configurations for each particle-ejection mode and take the average of $(X_C - X_C^0)/d_s$ or $(Y_C - Y_C^0)/d_s$ for the horizontal or vertical ejection mode as a function of ejection times $N = [1, 20]$ and shift distance $\delta = (0.5d_s, 2.0d_s, 3.5d_s)$.

We also record the average number of particles n being ejected at each N . The results are shown in Fig. 5.

As can be seen clearly in Fig. 5(a), without the interference from gravity, the three curves of $(X_C - X_C^0)/d_s$ are well separated and varying systematically, where the curve of $\delta = 0.5d_s$ with the strongest ejection strength on top, and the curve of $\delta = 3.5d_s$ with the weakest ejection strength at the bottom. On the other hand, as the ejection mode turns vertical, gravity comes into play by decelerating the cruiser during ejection against it, or accelerating the cruiser during ejection with it. The gravity effect complicates the kinetic response, and the mere effect of changing the ejection strength δ becomes less obvious. As a result, the three curves of $(Y_C - Y_C^0)/d_s$ are closer to one another, as shown in Fig. 5(b) and (c). The error bars in all three cases are somewhat large for two possible reasons: 1) The ejection directions of the shifted particles could be scattered, because we do not strictly control it and let the particle-cruiser interaction force \vec{f}_{ij}^n , defined in Eqn.(1), take care of it automatically. 2) The system only has about 4000 particles and the boundary effect from the container walls cannot be ignored easily. We plan to use a much larger system size in our next study to eliminate these artificial effects and to reduce the error bars. Lastly, as shown in the insets of Fig. 5, the systematic increasing of the average number of particles n being ejected at each N , as the particle-ejection strength δ decreases from $3.5d_s$ to $0.5d_s$, agrees with the trend of $(X_C - X_C^0)/d_s$ and $(Y_C - Y_C^0)/d_s$, where in general the cruiser can take in more pocketed particles if it ejects more forcefully.

D. Future work and related experimental setup

For future work, we plan to introduce interparticle friction into our MD simulation, and explore the stress distribution around the cruiser to extract the optimal geometry of the indent-region that offers the best propelling efficiency.

One great advantage of the simple design of the cruiser and the simulation setup is we can also verify our numerical results with corresponding experiments. The shifting of pocketed particles in the indent-region can be done either manually by hand or automatically by a machine. We can perform the particle-ejection using a mechanical device that expels the shifted particles using compressed air or a spring, or impact from a falling object transferring its gravitational potential energy to the kinetic energy of the ejected particles and the cruiser.

IV. CONCLUSIONS

In this study, we propose an extremely simple design of a fully-mobile cruiser in a 2D granular medium under gravity. The cruiser has an overall round shape except with a square indentation on its edge, measuring

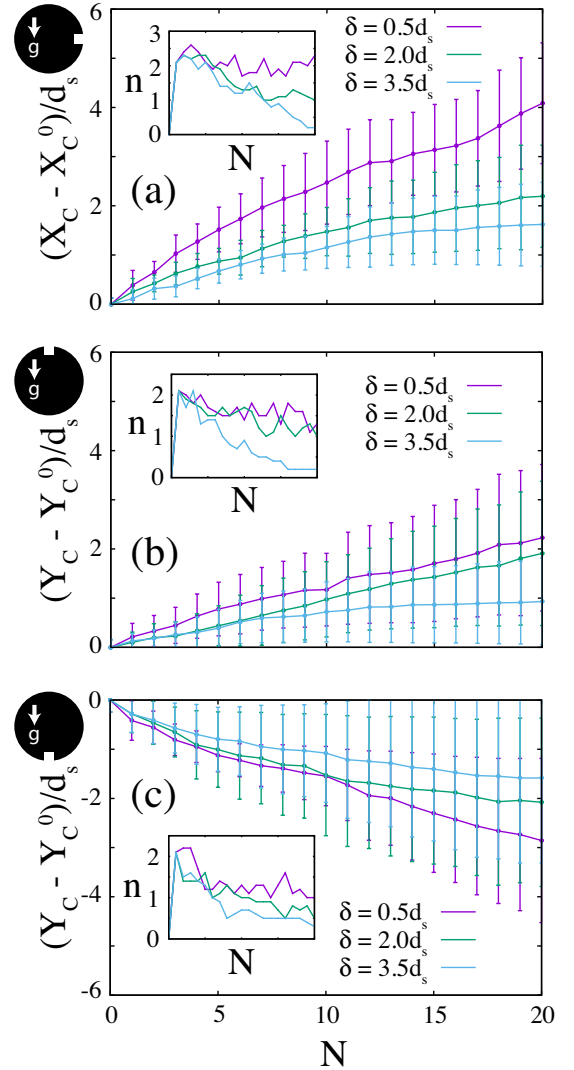


FIG. 5. (Color online) The normalized net displacement $(X_C - X_C^0)/d_s$ or $(Y_C - Y_C^0)/d_s$ for ejection mode (a) perpendicular to gravity, (b) against gravity or (c) with gravity as a function of ejection times $N = [1, 20]$ and shift distance $\delta = 0.5d_s$ (dark), $2.0d_s$ (medium) and $3.5d_s$ (light), respectively. The particle-ejection strength is inversely proportional to δ . The insets show the corresponding number of ejected particles n with the same horizontal axis. Each curve is obtained by averaging the results of ten different initial configurations.

two small particles wide and placed facing the designated motion direction. In addition to this simple shape, the cruiser can transfer the particles pocketed in the indent-region to its rear-half and eject them to obtain thrust for moving forward. The emptied indent-region offers necessary space to locally unjam the particles ahead of the cruiser and make room for it. We orient the indentation to one side of the cruiser to perform the horizontal particle-ejection mode perpendicular to gravity. For vertical particle-ejection modes against or with gravity, we put the indentation on the top of or at the bottom of the

cruiser.

Using MD simulations to study the kinetic response of the cruiser in a sea of nearly 50-50 bidisperse granular particles interacting via the purely repulsive linear spring force and velocity-dependent damping force, we identify three distinct phases during an particle-ejection: 1) Phase I starts from the beginning of the ejection until ejected particles completely leaving the cruiser. In this phase, the cruiser speeds up and reaches a maximum velocity while its displacement only increases slightly. 2) Phase II ends until the cruiser exhausts all of its momentum built up previously. In this phase, the cruiser keeps moving due to the inertial effects and obtains the longest displacement among all three phases. The cruiser eventually is stopped by the compressed particles in front of it. 3) Phase III is when the compressed particles start to push back until the system becomes fully relaxed again. At the end of this phase, the decompressed particles push the cruiser backwards but on average never back to its original position. We find the three phases exist uni-

versally in all three particle-ejection modes. Besides, we also verify the cruiser indeed can move smoothly perpendicular or parallel to gravity by successively ejecting pocketed particles, using the 'one steps forward, half step back' strategy containing the above three phases. The cruising efficiency increases proportionally to the ejection strength and works at its best if without the interference from gravity.

In summary, we believe the simplicity and the efficiency of our proposed cruiser offers important physics insights for an object moving within granular materials, and establish a solid base for engineering mobile objects in athermal media with practical applications in the visible future.

V. ACKNOWLEDGMENTS

GJG gratefully acknowledges financial support from Shizuoka University startup funding.

-
- [1] J. Aguilar, T. Zhang, F. Qian, M. Kingsbury, B. McInroe, N. Mazouchova, C. Li, R. Maladen, C. Gong, M. Travers, R. L. Hatton, H. Choset, P. B. Umbanhowar, and D. I. Goldman, *Rep. Prog. Phys.* **79**, 110001 (2016).
 - [2] H. M. Jaeger, S. R. Nagel, and R. P. Behringer, *Rev. Mod. Phys.* **68**, 1259 (1996).
 - [3] Y. Ding, N. Gravish, and D. I. Goldman, *Phys. Rev. Lett.* **106**, 028001 (2011).
 - [4] S. S. Sharpe, R. Kuckuk, and D. I. Goldman, *Phys. Biol.* **12**, 046009 (2014).
 - [5] H. Askari and K. Kamrin, *Nat. Mater.* **15**, 12741279 (2016).
 - [6] J. Slonaker, D. C. Motley, Q. Zhang, S. Townsend, C. Senatore, K. Iagnemma, and K. Kamrin, *Phys. Rev. E* **95**, 052901 (2017).
 - [7] Z. Peng, Y. Ding, K. Pietrzyk, G. J. Elfring, and O. S. Pak, *Phys. Rev. E* **96**, 012907 (2017).
 - [8] P. Lee, M. Tsai, I. Hsieh, P. Tseng, and G. J. Gao, *arXiv:1707.08716* (2018).
 - [9] T. Shimada, D. Kadau, T. Shinbrot, and H. J. Herrmann, *Phys. Rev. E* **80**, 020301 (2009).
 - [10] R. Maladen, Y. Ding, C. Li, and D. I. Goldman, *Science* **325**, 314 (2009).
 - [11] C. Li, T. Zhang, and D. I. Goldman, *Science* **339**, 1408 (2013).
 - [12] D. I. Goldman, *Reviews of Modern Physics* **86**, 943 (2014).
 - [13] H. C. Astley, C. Gong, J. Dai, M. Travers, M. M. Serrano, P. A. Vela, H. Choset, J. R. M. III, D. L. Hu, and D. I. Goldman, *Proc. Natl. Acad. Sci.* **03**, 1418965112 (2015).
 - [14] Z. Peng, O. S. Pak, and G. J. Elfring, *Phys. Fluids* **28**, 031901 (2016).
 - [15] J. M. Rieser, P. E. Schiebel, A. Pazouki, F. Qian, Z. Goddard, A. Zangwill, D. Negrut, and D. I. Goldman, *arXiv:1712.00136* (2018).
 - [16] C. Li, P. B. Umbanhowar, H. Komsuoglu, D. E. Koditschek, and D. I. Goldman, *Proc. Natl. Acad. Sci.* **106**, 3029 (2009).
 - [17] A. G. Winter, R. L. H. Deits, D. S. Dorsch, A. H. Slocum, and A. E. Hosoi, *Bioinspir. Biomim.* **9**, 036009 (2014).
 - [18] A. E. Hosoi and D. I. Goldman, *Annu. Rev. Fluid Mech.* **47**, 431 (2015).
 - [19] G. J. Gao, J. Blawdziewicz, C. S. O'Hern, and M. D. Shattuck, *Phys. Rev. E* **80**, 061304 (2009).